Editors' Suggestion

Range-separated hybrid functional pseudopotentials

Yang Yang [1,*] Georgia Prokopiou [2,*] Tian Qiu [3] Aaron M. Schankler [3] Andrew M. Rappe [3] Leeor Kronik [2] and Robert A. DiStasio, Jr. [1,†]

[1]*Department of Chemistry and Chemical Biology, Cornell University, Ithaca, New York 14853, USA*

[2]*Department of Molecular Chemistry and Materials Science, Weizmann Institute of Science, Rehovoth 76100, Israel*

[3]*Department of Chemistry, University of Pennsylvania, Philadelphia, Pennsylvania 19104, USA*

(Received 22 February 2023; accepted 22 June 2023; published 23 October 2023)

Consistency between the exchange-correlation (XC) functional used during pseudopotential construction and planewave-based electronic structure calculations is important for an accurate and reliable description of the structure and properties of condensed-phase systems. In this work, we present a general scheme for constructing pseudopotentials with range-separated hybrid (RSH) XC functionals based on the solution of the all-electron radial integro-differential equation for a spherically symmetrized reference atomic configuration. As a proof of principle, we demonstrate pseudopotential construction with the Perdew-Burke-Ernzerhof (PBE), hybrid PBE (PBE0), Heyd-Scuseria-Ernzerhof RSH (HSE06), and screened RSH (SRSH, based on the long-range corrected LC-ωPBE0 RSH) XC functionals for a select set of atoms and then investigate the importance of pseudopotential consistency when computing band gaps, equilibrium lattice parameters, bulk moduli, and atomization energies of several solid-state systems. In doing so, we find that pseudopotential consistency errors tend to be systematic and can be as large as 0.1 eV (or 1.4%) when computing band gaps.

DOI: 10.1103/PhysRevB.108.165142

I. INTRODUCTION

Density functional theory (DFT) [1,2] has long been the computational workhorse of first-principles calculations in the fields of physics, chemistry, and materials science [3–8]. DFT is an exact theory in principle, but as it requires an exchange-correlation (XC) functional that is generally unknown, it is almost always approximate in practice. A very large number of approximate XC functionals have been suggested to date, many of which can be categorized by classes of increasing accuracy and complexity using Perdew's five-rung "Jacob's ladder" scheme [9]. On the two lower rungs of this ladder lie the local density approximation (LDA) and generalized gradient approximation (GGA) (e.g., the Perdew-Burke-Ernzerhof (PBE) functional [10]), in which the XC term is an explicit functional of the density alone or the density and its gradient, respectively. The three higher rungs add orbital-dependent ingredients [11] of increasing sophistication, with third-rung functionals (i.e., meta-GGAs) also depending on the kinetic energy density and/or Laplacian of the density, fourth-rung functionals (e.g., hybrids) generally depending on the occupied orbitals, and fifth-rung functionals incorporating virtual/unoccupied orbital information.

Hybrid XC functionals, which employ a fraction of Fock exchange (or exact exchange) as one of their ingredients [12,13] (e.g., the hybrid PBE (PBE0) functional [14,15]), are among the most popular fourth-rung functionals, as they often offer an excellent balance between accuracy and computational cost [11]. Range-separated hybrids (RSHs) [16,17] are a special case of hybrid functionals, in which different fractions of Fock exchange are employed in different interelectron interaction ranges, thereby allowing for a finer balance between exchange and correlation components. Popular RSH functionals may include Fock exchange only in the short range (e.g., the Heyd-Scuseria-Ernzerhof (HSE06) functional [18], which will be referred to as HSE throughout this work), only in the long range (e.g., the long-range corrected PBE (LC-ωPBE) functional [19] and the Baer-Neuhauser-Livshits (BNL) functional [20]), or in both ranges (e.g., the long-range corrected PBE0 (LC-ωPBE0) functional [21], the Cambridge-adapted Becke-3-Lee-Yang-Parr (CAM-B3LYP) functional [22], and the Chai-Head-Gordon RSH functional based on Becke exchange (ωB97X) [23]). RSH functionals in which the parameters are chosen by optimal tuning, i.e., by a per-system selection of parameters that satisfy physical criteria, have also been shown to be of particular use for electronic and optical spectroscopy in both molecules [24] and solids [25].

Solid-state DFT calculations often employ the pseudopotential (PS) method (for an overview, see, e.g., Refs. [26–29] and references therein), which replaces the core electrons by an effective potential that describes their effect on the valence electrons. By removing the Coulomb singularity of the nuclear-electronic potential and eliminating the core electrons from explicit consideration, the PS method dramatically reduces the cost of solid-state DFT calculations. Clearly, a consistent level of theoretical treatment requires that the PS be generated using the same XC functional that is employed for the DFT calculation. However, virtually all PSs in everyday use are generated using the two lowest rungs of Jacob's ladder, namely, LDA and GGA. Given that the use of an inconsistent

*These authors contributed equally to this work.

†distasio@cornell.edu

PS has been shown to introduce uncontrolled PS consistency errors (PSCEs) even between LDA and GGA [30], this is a potentially serious issue that needs to be addressed when performing more computationally intensive (and higher accuracy) DFT calculations with higher-rung XC functionals. Only recently have schemes for constructing PSs for third- and fourth-rung functionals (i.e., meta-GGAs and hybrids) been reported in the literature along with an evaluation of the associated PSCEs [31–33]. To the best of our knowledge, PS schemes for generating fourth-rung RSH functionals have not been developed or studied to date.

In this work, we remedy this situation. We present the general process and basic equations for the construction of RSH-type PSs. Specifically, we derive the all-electron RSH radial integro-differential equation by utilizing the Slater configuration-averaging scheme [32,34,35] in conjunction with a multipole expansion of the short-range Coulomb repulsion kernel [36]. We then show how RSH-type PSs are constructed from the all-electron orbitals and potentials. To make the entire process clear, we also show how this approach is implemented in practice (within the OPIUM code [37]). Finally, we illustrate the importance of these PSs by critically assessing the PSCEs when computing band gaps, equilibrium lattice parameters, bulk moduli, and atomization energies of several solid-state systems. In doing so, we find that PSCEs tend to be systematic and can be as large as 1.4% when computing these properties using fourth-rung RSH XC functionals.

II. THEORY

A. Overview of RSH functionals

The exchange (x) energy of an RSH XC functional is split into long-range (LR) and short-range (SR) terms [17], often using the error function [22] with a range-separation parameter μ. The XC energy, $E_{\rm xc}^{\rm RSH} = E_{{\rm x},\mu}^{\rm RSH} + E_{\rm c}^{\rm DFA}$, is then written as

$$\begin{aligned} E_{\rm xc}^{\rm RSH} =& \alpha E_{{\rm SR},\mu}^{\rm Fock} + (1-\alpha) E_{{\rm SR},\mu}^{\rm DFA} + (\alpha+\beta) E_{{\rm LR},\mu}^{\rm Fock} \\ &+ (1-\alpha-\beta) E_{{\rm LR},\mu}^{\rm DFA} + E_{\rm c}^{\rm DFA}, \end{aligned} \tag{1}$$

where DFA denotes the employed density functional approximation (e.g., PBE). In the general RSH scheme, α, β, and μ are free parameters (various choices of which are discussed below), and the SR- and LR-Fock terms are given by

$$\begin{aligned} E_{{\rm SR},\mu}^{\rm Fock} =& -\sum_{ij} \int d\boldsymbol{r}\, d\boldsymbol{r}'\, \psi_i^*(\boldsymbol{r}) \psi_j(\boldsymbol{r}) \\ &\times \frac{\operatorname{erfc}(\mu|\boldsymbol{r}-\boldsymbol{r}'|)}{|\boldsymbol{r}-\boldsymbol{r}'|} \psi_j^*(\boldsymbol{r}') \psi_i(\boldsymbol{r}') \end{aligned} \tag{2}$$

and

$$\begin{aligned} E_{{\rm LR},\mu}^{\rm Fock} =& -\sum_{ij} \int d\boldsymbol{r}\, d\boldsymbol{r}'\, \psi_i^*(\boldsymbol{r}) \psi_j(\boldsymbol{r}) \\ &\times \frac{\operatorname{erf}(\mu|\boldsymbol{r}-\boldsymbol{r}'|)}{|\boldsymbol{r}-\boldsymbol{r}'|} \psi_j^*(\boldsymbol{r}') \psi_i(\boldsymbol{r}'), \end{aligned} \tag{3}$$

where ψ_i and ψ_j are the occupied wave functions (orbitals). Note that for simplicity here and throughout, we consider only closed-shell systems; hence, a factor of $1/2$ is not included in Eqs. (2) and (3).

Like all hybrids, RSH functionals are almost invariably employed within the generalized Kohn-Sham (GKS) scheme [38], i.e., using a nonmultiplicative exchange potential related to the Fock operator. The corresponding XC potential, $\hat{V}_{\rm xc}^{\rm RSH} = \hat{V}_{\rm x} + V_{\rm c}^{\rm DFA}(\rho(\boldsymbol{r}))$, is then

$$\begin{aligned} \hat{V}_{\rm xc}^{\rm RSH} =& \alpha \hat{V}_{{\rm SR},\mu}^{\rm Fock} + (1-\alpha) V_{{\rm SR},\mu}^{\rm DFA}(\rho(\boldsymbol{r})) + (\alpha+\beta) \hat{V}_{{\rm LR},\mu}^{\rm Fock} \\ &+ (1-\alpha-\beta) V_{{\rm LR},\mu}^{\rm DFA}(\rho(\boldsymbol{r})) + V_{\rm c}^{\rm DFA}(\rho(\boldsymbol{r})), \end{aligned} \tag{4}$$

where the hat signifies a nonmultiplicative operator and $\rho(\boldsymbol{r})$ is the electron density. As an example, if we choose PBE for the DFA (i.e., the use of the PBE correlation functional in conjunction with the SR and LR versions of PBE exchange [39,40]), then setting $\alpha = 0.25$, $\beta = -0.25$, and $\mu = 0.11$ bohr^{-1} leads to the HSE functional [18].

B. All-electron calculation

The first step in constructing a PS is to solve the all-electron (AE) GKS equation for a spherically symmetrized *reference* atomic configuration, from which central angular-momentum-dependent PSs can be generated. Specifically, we solve

$$\left[-\tfrac{1}{2}\nabla^2 + V_{\rm ion} + V_{\rm H} + \hat{V}_{\rm xc}\right] \psi_{nlm}(\boldsymbol{r}) = \epsilon_{nlm} \psi_{nlm}(\boldsymbol{r}), \tag{5}$$

where the terms in the square brackets are the electron kinetic energy operator, the nuclear-electron attraction potential, the classical electron-electron repulsion (Hartree) potential, and the XC potential, respectively. In this expression, $\psi_{nlm}(\boldsymbol{r})$ and ϵ_{nlm} are the wave function and eigenvalue associated with the nlm quantum numbers, respectively.

The atomic wave functions $\psi_{nlm}(\boldsymbol{r})$ can be written as

$$\psi_{nlm}(\boldsymbol{r}) = \frac{\phi_{nl}(r)}{r} Y_{lm}(\theta, \varphi), \tag{6}$$

where $\phi_{nl}(r)/r$ is the (normalized) radial part of the wave function and $Y_{lm}(\theta, \varphi)$ is a spherical harmonic, with the aim of simplifying Eq. (5) into a one-dimensional ordinary differential equation for the radial function $\phi_{nl}(r)$. However, the presence of Fock exchange in $\hat{V}_{\rm xc}$ complicates this radial transformation, as the evaluation of this contribution depends on the magnetic quantum number m, which reintroduces an angular dependence. To overcome this issue and enforce spherical symmetry, we use the concept of the "average energy of configuration" introduced by Slater [34] to remove the angular dependence. This so-called Slater configuration-averaging (SCA) scheme, which was used successfully to deal with the standard/full-range (FR) Fock exchange in the context of constructing PSs for global hybrid functionals [32], is explained in more detail in Secs. I A–I C and II A of the accompanying Supplemental Material [41].

For a global hybrid, in which $\hat{V}_{\rm xc} = \hat{V}_{\rm x} + V_{\rm c}^{\rm DFA}(\rho(\boldsymbol{r})) = \alpha \hat{V}_{\rm FR}^{\rm Fock} + (1-\alpha) V_{\rm x}^{\rm DFA}(\rho(\boldsymbol{r})) + V_{\rm c}^{\rm DFA}(\rho(\boldsymbol{r}))$, this procedure leads to the following *radial* expression for the (FR-)Fock

contribution:

$$\hat{V}_{\rm FR}^{\rm Fock}\phi_{nl}(r) = \frac{1}{r}\Bigg[\sum_{L=0}^{2l} A^{\rm FR}_{nl,nl,L} Y^L(nl,nl;r)\phi_{nl}(r) + \sum_{n'l'\neq nl}\sum_{L=|l-l'|}^{l+l'} B^{\rm FR}_{nl,n'l',L} Y^L(nl,n'l';r)\phi_{n'l'}(r)\Bigg], \tag{7}$$

in which

$$Y^L(nl,n'l';r) \equiv \int_0^r dr' \left(\frac{r'}{r}\right)^L \phi^*_{nl}(r')\phi_{n'l'}(r') + \int_r^\infty dr' \left(\frac{r}{r'}\right)^{L+1} \phi^*_{nl}(r')\phi_{n'l'}(r') \tag{8}$$

and $A^{\rm FR}_{nl,nl,L}$ and $B^{\rm FR}_{nl,n'l',L}$ are the expansion coefficients corresponding to exchange interactions between equivalent ($nl = n'l'$) and nonequivalent ($nl \neq n'l'$) electrons, respectively; explicit expressions for both are given by Eqs. (III.13) and (III.16) in the Supplemental Material [41]. In this work, we use the Y^L symbol [as defined in Eq. (8)] for consistency with the notation in Ref. [35], which should not be confused with the Y_{lm} symbol used to denote the spherical harmonics in Eq. (6).

To take full advantage of these results for the FR-Fock operator in the context of RSH functionals, the terms in Eq. (4) can be rearranged as follows:

$$\hat{V}_{\rm xc}^{\rm RSH} = (\alpha+\beta)\hat{V}_{\rm FR}^{\rm Fock} - \beta\hat{V}_{{\rm SR},\mu}^{\rm Fock} + \beta V_{{\rm SR},\mu}^{\rm DFA}(\rho(\boldsymbol{r})) + (1-\alpha-\beta)V_{\rm FR}^{\rm DFA}(\rho(\boldsymbol{r})) + V_{\rm c}^{\rm DFA}(\rho(\boldsymbol{r})), \tag{9}$$

such that the only term that needs to be addressed is $\hat{V}_{{\rm SR},\mu}^{\rm Fock}$, i.e., the SR-Fock contribution. Here, we note that Eqs. (7) and (8) are based on a multipole expansion of the standard $1/|\boldsymbol{r}-\boldsymbol{r'}|$ operator found in FR-Fock exchange [see Eqs. (I.6) and (I.7) in the Supplemental Material] [41]. To evaluate the $\hat{V}_{{\rm SR},\mu}^{\rm Fock}$ contribution in Eq. (9), we need to consider the analogous expansion for the $\mathrm{erfc}(\mu|\boldsymbol{r}-\boldsymbol{r'}|)/|\boldsymbol{r}-\boldsymbol{r'}|$ operator found in the SR-Fock exchange term in Eq. (2). Such an expansion was studied in detail by Ángyán *et al.* [36] (and used successfully by Lehtola [42] to calculate fractionally occupied atoms) and is given as

$$\frac{\mathrm{erfc}(\mu|\boldsymbol{r}-\boldsymbol{r'}|)}{|\boldsymbol{r}-\boldsymbol{r'}|} = \sum_{L=0}^{\infty} \mathcal{F}_L(r,r',\mu)P_L(\cos\gamma), \tag{10}$$

where $P_L(\cos\gamma)$ is an Lth-order Legendre polynomial, γ is the angle between $\boldsymbol{r}$ and $\boldsymbol{r'}$, and $\mathcal{F}_L(r,r',\mu) = \mu\Phi_L(\mu r_<, \mu r_>)$ are radial expansion functions [where $r_< = \min(r,r')$ and $r_> = \max(r,r')$]; see Sec. II B in the Supplemental Material for more details [41].

With Eq. (10) in hand, one can now apply the SCA procedure to derive the SR analogs of Eqs. (7) and (8); see Sec II B in the Supplemental Material for a detailed derivation [41]. In doing so, we obtained the following *radial* expression for the SR-Fock contribution:

$$\hat{V}_{{\rm SR},\mu}^{\rm Fock}\phi_{nl}(r) = \frac{1}{r}\Bigg[\sum_{L=0}^{2l} A^{\rm SR}_{nl,nl,L}\mathcal{Z}^L_\mu(nl,nl;r)\phi_{nl}(r) + \sum_{n'l'\neq nl}\sum_{L=|l-l'|}^{l+l'} B^{\rm SR}_{nl,n'l',L}\mathcal{Z}^L_\mu(nl,n'l';r)\phi_{n'l'}(r)\Bigg] \tag{11}$$

in which

$$\mathcal{Z}^L_\mu(nl,n'l';r) \equiv \mu r\int_0^r dr' \Phi_L(\mu r',\mu r)\phi^*_{nl}(r')\phi_{n'l'}(r') + \mu r\int_r^\infty dr' \Phi_L(\mu r,\mu r')\phi^*_{nl}(r')\phi_{n'l'}(r') \tag{12}$$

and $A^{\rm SR}_{nl,nl,L}$ and $B^{\rm SR}_{nl,n'l',L}$ are the corresponding SR expansion coefficients given by Eqs. (III.13) and (III.16) in the Supplemental Material [41].

Using these expressions, Eq. (5) can now be transformed into the following Slater-averaged all-electron RSH radial integro-differential equation:

$$\begin{aligned}\frac{d^2\phi_{nl}(r)}{dr^2} = \frac{2}{r}\Bigg[&\frac{l(l+1)}{2r} - Z + Y_\mu(nl;r) \\ &+ (1-\alpha-\beta)rV_{\rm FR}^{\rm DFA}(r) \\ &+ \beta r V_{{\rm SR},\mu}^{\rm DFA}(r) + rV_{\rm c}^{\rm DFA}(r)\Bigg]\phi_{nl}(r) \\ &+ \frac{2}{r}[(\alpha+\beta)X_{\rm FR}(nl;r) - \beta X_{{\rm SR},\mu}(nl;r)] \\ &+ \epsilon_{nl}\phi_{nl}(r);\end{aligned} \tag{13}$$

see Sec. III A in the Supplemental Material for more details [41]. In this expression, $Y_\mu(nl;r)$ contains the Hartree (H) contribution as well as the equivalent-electron ($nl = n'l'$) exchange contributions in the FR- and SR-Fock terms via Eqs. (7) and (11), namely,

$$\begin{aligned}Y_\mu(nl;r) \equiv &\sum_{n'l'}\sum_{L=|l-l'|}^{l+l'} A^{\rm H}_{nl,n'l',L}Y^L(n'l',n'l';r) \\ &+ (\alpha+\beta)\sum_{L=0}^{2l} A^{\rm FR}_{nl,nl,L}Y^L(nl,nl;r) \\ &- \beta\sum_{L=0}^{2l} A^{\rm SR}_{nl,nl,L}\mathcal{Z}^L_\mu(nl,nl;r),\end{aligned} \tag{14}$$

where $A^{\rm H}_{nl,n'l',L}$ are the needed expansion coefficients given by Eq. (III.12) in the Supplemental Material [41]. In Eq. (13), $X_{\rm FR}(nl;r)$ and $X_{{\rm SR},\mu}(nl;r)$ are the corresponding nonequivalent-electron ($nl \neq n'l'$) exchange contributions from the FR- and SR-Fock terms in Eqs. (7) and (11), respectively:

$$X_{\rm FR}(nl;r) \equiv \sum_{n'l'\neq nl}\sum_{L=|l-l'|}^{l+l'} B^{\rm FR}_{nl,n'l',L}Y^L(nl,n'l';r)\phi_{n'l'}(r) \tag{15}$$

and

$$X_{\mathrm{SR},\mu}(nl;r) \equiv \sum_{n'l'\neq nl} \sum_{L=|l-l'|}^{l+l'} B^{\mathrm{SR}}_{nl,n'l',L} \mathcal{Z}^{L}_{\mu}(nl,n'l';r)\phi_{n'l'}(r). \tag{16}$$

Detailed expressions for the remaining FR- and SR-DFA exchange potentials in $\hat{V}^{\mathrm{RSH}}_{\mathrm{xc}}$ [i.e., $V^{\mathrm{DFA}}_{\mathrm{FR}}(\rho(\boldsymbol{r}))$ and $V^{\mathrm{DFA}}_{\mathrm{SR},\mu}(\rho(\boldsymbol{r}))$ in Eq. (9)] are provided in Sec. III B in the Supplemental Material [41].

C. Pseudopotential generation

In this work, we construct RSH-type PSs according to the norm-conserving PS method [43]. With the set of radial AE functions $\{\phi_{nl}(r)\}$ for a preselected reference atomic configuration in hand [obtained by finding the solutions to Eq. (13)], this procedure starts with generating a corresponding set of radial pseudofunctions $\{\widetilde{\phi}_{nl}(r)\}$ for the valence electrons. Each $\widetilde{\phi}_{nl}(r)$ is constructed to be nodeless and slowly varying for $r < r_{\mathrm{c}}$ (a user-defined cutoff radius) with $\widetilde{\phi}_{nl}(r) = \phi_{nl}(r)$ for $r \geqslant r_{\mathrm{c}}$, subject to the constraint that the norm of $\widetilde{\phi}_{nl}(r)$ equals that of $\phi_{nl}(r)$. The procedure to generate a valid and smooth radial pseudofunction is nonunique and several protocols, e.g., those described in Refs. [44–47], are widely used today. In this work, we use the optimized PS approach of Rappe *et al.* [44], but all considerations outlined herein are applicable to other choices as well.

Once $\widetilde{\phi}_{nl}(r)$ are constructed, the so-called unscreened semilocal (SL) term in the PS, $V^{\mathrm{SL}}_{l}(r)$, is obtained by inverting Eq. (13) and then subtracting the Hartree and XC contributions corresponding to the valence electrons [48]. $V^{\mathrm{SL}}_{l}(r)$ generated from functionals that include nonlocal Fock exchange (e.g., global hybrids and RSH functionals) will exhibit a "non-Coulombic tail" arising from this unscreening procedure [49]; in this work, this issue is remedied by the smoothing procedure suggested by Trail and Needs [48,50], which (following the work of Engel *et al.* [49] for optimized effective potentials) unscreens the PS in a way that slightly sacrifices perfect norm conservation but restores the correct asymptotic potential. To improve transferability, we also employed the designed-nonlocal (DNL) method [51–53], which adds an auxiliary function, $A(r)$ (the so-called local augmentation operator), to the Kleinman-Bylander (KB) separable form [54] for the PS:

$$V^{\mathrm{PS}}(\boldsymbol{r}) = V^{\mathrm{loc}}(r) + A(r) + \sum_{lm} \frac{|\Delta V_l(r)\,\widetilde{\psi}_{nlm}(\boldsymbol{r})\rangle\langle\widetilde{\psi}_{nlm}(\boldsymbol{r})\Delta V_l(r)|}{\langle\widetilde{\psi}_{nlm}(\boldsymbol{r})|\Delta V_l(r)|\widetilde{\psi}_{nlm}(\boldsymbol{r})\rangle}. \tag{17}$$

In this expression, $V^{\mathrm{loc}}(r)$ is the local component of the PS, which was set equal to $V^{\mathrm{SL}}_{0}(r)$ throughout this work (i.e., the default choice in OPIUM),

$$\Delta V_l(r) \equiv V^{\mathrm{SL}}_{l}(r) - V^{\mathrm{loc}}(r) - A(r), \tag{18}$$

and $\widetilde{\psi}_{nlm}(\boldsymbol{r}) = [\widetilde{\phi}_{nl}(r)/r]Y_{lm}(\theta,\varphi)$ is the pseudo wave function generated for the reference atomic configuration [i.e., the analog of the AE atomic wave function in Eq. (6)]. For $A(r) = 0$, we note that Eq. (17) simplifies to the standard KB form [54]. As mentioned above, $A(r)$ can be optimized to improve transferability (see below and Sec. IV A in the Supplemental Material for more details [41]). We also note that our work inherits both the strengths and weaknesses of the KB approach augmented with the aforementioned smoothing procedure. Specifically, the RSH-type PS introduced in this work (like all KB PSs), can be susceptible to "ghost states," i.e., to the appearance of spurious one-node solutions below the zero-node state [55,56]. Within the scope of this work, we have employed standard tests for detecting such states [55,56] and have not encountered particular difficulties with this issue.

To assess the transferability of $V^{\mathrm{PS}}(\boldsymbol{r})$, an AE calculation on a *test* (i.e., nonreference) atomic configuration is performed by solving Eq. (13) to obtain $\{\phi^{\mathrm{test}}_{nl}(r)\}$ and $\{\epsilon^{\mathrm{test}}_{nl}\}$. These quantities are then compared to the corresponding radial pseudofunctions and eigenvalues, $\widetilde{\phi}^{\mathrm{test}}_{nl}(r)$ and $\widetilde{\epsilon}^{\mathrm{test}}_{nl}$, for the test atomic configuration. To enable this comparison, $V_{\mathrm{ion}}(\rho(\boldsymbol{r}))$ in Eq. (5) is replaced with $V^{\mathrm{PS}}(\boldsymbol{r})$ from Eq. (17) to yield the following equation for $\widetilde{\psi}^{\mathrm{test}}_{nlm}(\boldsymbol{r})$ and $\widetilde{\epsilon}^{\mathrm{test}}_{nlm}$:

$$\left[-\frac{1}{2}\nabla^2 + V^{\mathrm{PS}}(\boldsymbol{r}) + V_{\mathrm{H}}(\widetilde{\rho}^{\,\mathrm{test}}(\boldsymbol{r})) + \hat{V}_{\mathrm{xc}}\right]\widetilde{\psi}^{\mathrm{test}}_{nlm}(\boldsymbol{r}) = \widetilde{\epsilon}^{\mathrm{test}}_{nlm}\widetilde{\psi}^{\mathrm{test}}_{nlm}(\boldsymbol{r}), \tag{19}$$

where $\widetilde{\rho}^{\,\mathrm{test}}(\boldsymbol{r})$ is the electron density formed from the valence pseudo wave functions of the test configuration. Following the SCA procedure for RSH functionals described above in Sec. II B, we arrive at the needed RSH radial integro-differential equation [i.e., the analog of Eq. (13)] for $\widetilde{\phi}^{\mathrm{test}}_{nl}(r)$:

$$\begin{aligned}\frac{d^2\widetilde{\phi}^{\mathrm{test}}_{nl}(r)}{dr^2} = \frac{2}{r}\Bigg[&\frac{l(l+1)}{2r} - r[V^{\mathrm{loc}}(r) + A(r)] + Y_{\mu}(nl;r) \\ &+ (1-\alpha-\beta)rV^{\mathrm{DFA}}_{\mathrm{FR}}(r) \\ &+ \beta r V^{\mathrm{DFA}}_{\mathrm{SR},\mu}(r) + rV^{\mathrm{DFA}}_{\mathrm{c}}(r)\Bigg]\widetilde{\phi}^{\mathrm{test}}_{nl}(r) \\ &+ \frac{2}{r}\Bigg[(\alpha+\beta)X_{\mathrm{FR}}(nl;r) - \beta X_{\mathrm{SR},\mu}(nl;r)\Bigg] \\ &- 2\frac{\int_0^{\infty} dr\,\widetilde{\phi}_{nl}(r)\Delta V_l(r)\widetilde{\phi}^{\mathrm{test}}_{nl}(r)}{\int_0^{\infty} dr\,\widetilde{\phi}_{nl}(r)\Delta V_l(r)\widetilde{\phi}_{nl}(r)}\Delta V_l(r)\widetilde{\phi}_{nl}(r) \\ &+ \widetilde{\epsilon}^{\mathrm{test}}_{nl}\widetilde{\phi}^{\mathrm{test}}_{nl}(r),\end{aligned} \tag{20}$$

where $\widetilde{\phi}_{nl}(r)$ corresponds to the radial pseudofunctions of the reference atomic configuration. Here, we note that the angular part of Eq. (17) is integrated out during the SCA procedure, and the Hartree and XC terms (i.e., Y_{μ}, $V^{\mathrm{DFA}}_{\mathrm{FR}}$, $V^{\mathrm{DFA}}_{\mathrm{SR},\mu}$, $V^{\mathrm{DFA}}_{\mathrm{c}}$, X_{FR}, and $X_{\mathrm{SR},\mu}$) are computed using the valence radial pseudofunctions from the test configuration [51–53]. We also note in passing that Eq. (20) for $\widetilde{\phi}^{\mathrm{test}}_{nl}(r) = \widetilde{\phi}_{nl}(r)$ (i.e., the trivial case in which the test configuration is the reference configuration) simplifies to an integro-differential equation for $\widetilde{\phi}_{nl}(r)$ [via algebraic manipulations of Eq. (20), Eq. (18), and the definition of $V^{\mathrm{SL}}_{l}(r)$]. In the standard case where $\widetilde{\phi}^{\mathrm{test}}_{nl}(r) \neq \widetilde{\phi}_{nl}(r)$, $A(r)$ will influence the generated $\widetilde{\phi}^{\mathrm{test}}_{nl}(r)$ and $\widetilde{\epsilon}^{\mathrm{test}}_{nl}$, and can therefore be used to improve transferability [51–53].

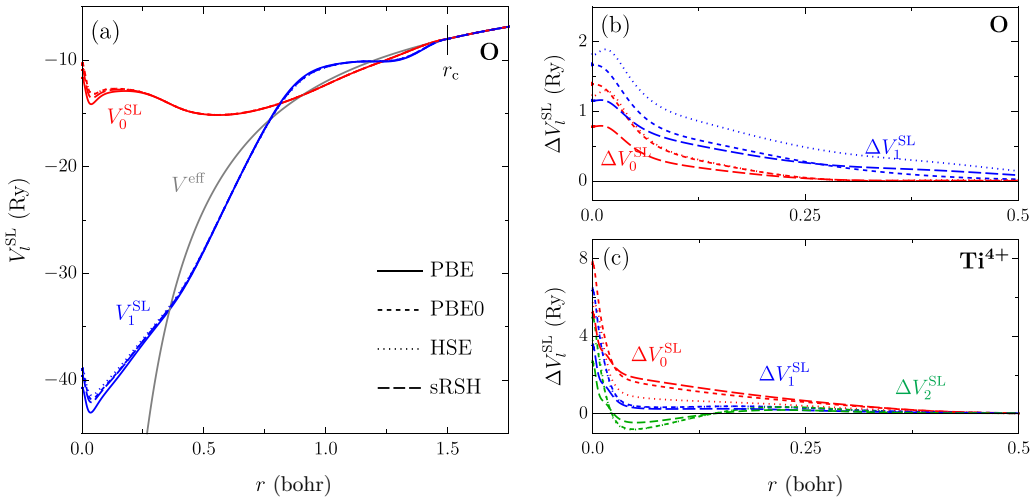

FIG. 1. (a) Plot of the unscreened semilocal PS term V_l^{SL} ($l = 0, 1$) versus r for the O atom generated with the PBE, PBE0, HSE, and SRSH DFAs. The effective external potential, $V^{\mathrm{eff}}(r) = -2Z_{\mathrm{eff}}/r \equiv -2(Z - Z_{\mathrm{core}})/r$, and cutoff radius r_c are also shown. For clarity, plots of $\Delta V_l^{\mathrm{SL}}(r) \equiv V_l^{\mathrm{SL,DFA}}(r) - V_l^{\mathrm{SL,PBE}}(r)$ for the PBE0, HSE, and SRSH DFAs are also depicted for (b) O ($l = 0, 1$) and (c) Ti^{4+} ($l = 0, 1, 2$).

D. Implementation

To enable AE and PS calculations involving RSH functionals, the following changes were made to OPIUM (version 4.1) [32]:

(1) To correctly account for the partial cancellation of self Hartree and Fock exchange interactions, we derived and implemented an extension to the SCA procedure for RSH functionals (see Sec. II in the Supplemental Material [41] for more details).

(2) Ángyán *et al.* [36] suggested a nonseparable analytical expansion (NSAE) as well as a separable series expansion (SSE) for $\mathcal{F}_L(r, r', \mu)$, the radial expansion functions in Eq. (10). However, Yang *et al.* [57] found that the accuracy of the SSE deteriorates with increasing angular momentum and distance (i.e., for large $r_>$) due to numerical precision issues. Hence, higher-precision (i.e., beyond customary double precision) data storage and evaluation would be needed to obtain an accurate representation for $\mathcal{F}_L(r, r', \mu)$ using the SSE. In the same breath, the NSAE suffers from numerical stability issues at short distances (i.e., for small $r_>$) [36]. In this work, we compensate for both of these shortcomings by using the NSAE for large $r_>$ and the SSE for small $r_>$ (see Sec. II B in the Supplemental Material [41] and Ref. [57] for more details).

(3) For the $V_{\mathrm{SR},\mu}^{\mathrm{DFA}}(r)$ term in Eq. (13), we have implemented the ωPBE exchange functional in OPIUM (see Refs. [39,40] and Sec. III B in the Supplemental Material [41]). This enables us to perform AE and PS calculations in OPIUM for ωPBE-based RSH functionals (e.g., HSE and screened-RSH (SRSH) [25] functionals).

(4) We have also enabled AE and PS calculations in OPIUM for Yukawa-based variants of these RSH functionals (see Refs. [58–61] and Sec. III B in the Supplemental Material [41]).

(5) We have also extended the DNL method in OPIUM to PS calculations involving Fock exchange [i.e., Eq. (20) for Hartree-Fock (HF), global hybrids, and RSH functionals].

For simplicity, the formalism presented in this work is nonrelativistic. While a relativistic treatment is outside the scope of this work, all PS comparisons below are fair, as nonrelativistic calculations are used for both consistent and inconsistent DFA/PS combinations.

III. RESULTS AND DISCUSSION

A. PS construction

We generated PSs in OPIUM for N, O, Mg^{2+}, Al^{+}, P, and Ti^{4+} with the PBE, PBE0, HSE, and SRSH [25,62] DFAs (see Secs. IV A–IV B in the Supplemental Material [41] for the parameters used during PS construction and SRSH calculations). Note that all RSH results reported in this work were generated using the error-function kernel in Eq. (10). In Fig. 1(a), we plot $V_l^{\mathrm{SL}}(r)$, the unscreened semilocal PS term, for $l = 0, 1$ for the O atom generated with these four DFAs. In general, the PSs corresponding to these four DFAs are quite similar and display more pronounced differences near the core ($r \lesssim 0.5$ bohr). For this reason, we also plot $\Delta V_l^{\mathrm{SL}}(r) \equiv V_l^{\mathrm{SL,DFA}}(r) - V_l^{\mathrm{SL,PBE}}(r)$ for the PBE0, HSE, and SRSH DFAs for O ($l = 0, 1$) and Ti^{4+} ($l = 0, 1, 2$) in Figs. 1(b) and 1(c), respectively. While there are general discernible trends that hold for both O and Ti^{4+}, we find that the largest differences among these PSs are at $r = 0$ and range from 1.3 Ry to 2.2 Ry for O and 2.8 Ry to 7.9 Ry for Ti^{4+}. As mentioned above, we employed the DNL approach to improve the transferability of the PS generated in this work. This was done by optimizing $A(r)$ in Eqs. (17) and (18) to minimize the (magnitudes of the) eigenvalue differences, $\Delta\epsilon \equiv \epsilon^{\mathrm{AE}} - \epsilon^{\mathrm{PS}}$, for a select set of orbitals and configurations of a given atom. As an illustration of this approach, we optimized $A(r)$ for the $3s, 3p, 3d, 4s$, and $4p$ orbitals across five different configurations of Ti^{p+}, ranging from $Ti^{4+} = [\mathrm{Ar}]$ (reference configuration) to $Ti^{2+} = [\mathrm{Ar}]3d^2$. In Fig. 2, we plot $\Delta\epsilon$ for these orbitals and configurations calculated using the DNL [optimized $A(r)$] and KB [$A(r) = 0$] approaches at the HSE

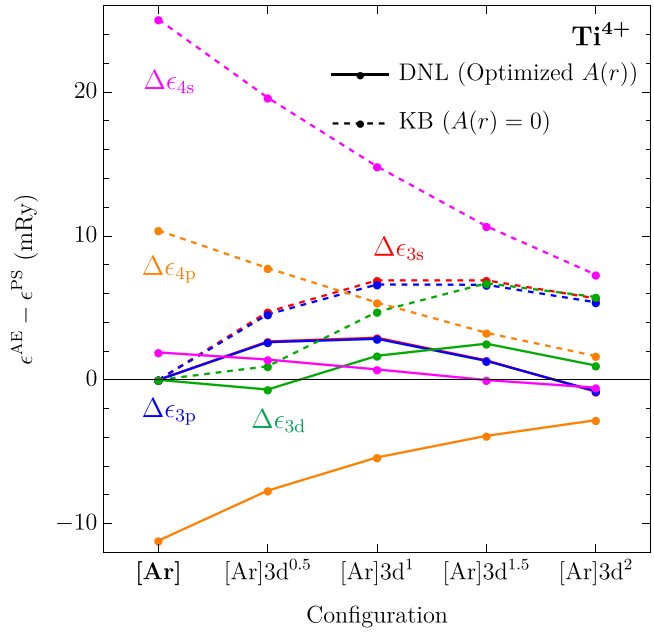

FIG. 2. Eigenvalue differences, $\Delta\epsilon \equiv \epsilon^{\mathrm{AE}} - \epsilon^{\mathrm{PS}}$, of the $3s$, $3p$, $3d$, $4s$, and $4p$ orbitals for different configurations of Ti^{p+} ($2 \leqslant p \leqslant 4$; reference configuration: $\mathrm{Ti}^{4+} = [\mathrm{Ar}]$) calculated using the DNL and standard KB approaches at the HSE level.

level. As expected, $\Delta\epsilon = 0$ for *any* $A(r)$ when considering the orbitals used during PS construction (i.e., $3s$, $3p$, $3d$) of the reference Ti^{4+} configuration [see discussion below Eq. (20)]. We find that when compared to the standard KB approach, the DNL optimization results in markedly improved $\Delta\epsilon_{3\mathrm{s}}$, $\Delta\epsilon_{3\mathrm{p}}$, and $\Delta\epsilon_{3\mathrm{d}}$ values for the remaining four test configurations, which is strongly indicative of improved PS transferability. For the outer unoccupied $4s$ orbital, which was included in the optimization of $A(r)$ (but not during PS construction), we also find a significant reduction in $\Delta\epsilon$ for all configurations. In the reference configuration alone, $\Delta\epsilon_{4\mathrm{s}}$ decreases from $\approx$25 mRy (KB) to $\approx$2 mRy (DNL); this tenfold error reduction is another criterion for demonstrating PS transferability. For the higher-lying $4p$ orbital, the DNL and KB approaches yielded very similar results.

B. PS consistency errors

Naturally, the next question to ask concerns the degree to which the differences among the PSs generated with the PBE, PBE0, HSE, and SRSH DFAs affect computed solid-state properties. To answer this question, we first computed the band gaps of MgO, AlN, TiO_2, and AlP with PBE, PBE0, HSE, and SRSH using an in-house modified version of Quantum ESPRESSO (version 6.6) [63] (see Sec. IV C in the Supplemental Material [41] for computational details). For each of the hybrid and RSH DFAs, we performed two calculations to quantify the PS consistency errors (PSCEs) in the band gap, i.e., the difference in a given solid-state property when computed using an *inconsistent* DFA/PS combination (e.g., a solid-state calculation employing PBE0 as the DFA in conjunction with a PBE PS) versus a *consistent* DFA/PS combination (e.g., a solid-state calculation employing PBE0 as the DFA in conjunction with a PBE0 PS). From the results shown in Table I, we find that the PSCEs grow with the magnitude of the band gap. As such, larger band gap materials (e.g., MgO and AlN) seem to be more sensitive to PS consistency (with average PSCEs of -1.3% (or 0.1 eV) and -0.8% (or 0.05 eV) for MgO and AlN, respectively), while smaller band gap systems (e.g., TiO_2 and AlP) are less affected by PS consistency (with average PSCEs of -0.1% and 0.3%, respectively). For MgO, AlN, and TiO_2, the PSCEs tend to be systematically negative (i.e., the use of consistent DFA/PS combinations tends to yield larger band gaps), while we see the opposite trend in AlP; hence, inconsistent DFA/PS combinations can lead to uncontrolled error. We also note in passing that the magnitudes of these errors do not seem to depend strongly on the choice of hybrid or RSH DFA.

TABLE I. Band gaps (eV) of select materials computed using consistent and inconsistent DFA/PS combinations. Absolute and relative PS consistency errors (PSCEs; bold font) were computed as band gap differences between inconsistent and consistent DFA/PS combinations (i.e., PBE0/PBE versus PBE0/PBE0).

DFA/PS	MgO ($\Gamma\to\Gamma$)	AlN ($\Gamma\to\Gamma$)	TiO_2 ($\Gamma\to\Gamma$)	AlP ($\Gamma\to X$)
PBE/PBE	4.551	4.305	1.766	1.612
PBE0/PBE	6.941	6.349	3.974	2.969
PBE0/PBE0	7.033	6.396	3.981	2.965
PSCEs	**−0.092** **−1.3%**	**−0.046** **−0.7%**	**−0.007** **−0.2%**	**0.004** **0.1%**
HSE/PBE	6.226	5.650	3.237	2.313
HSE/HSE	6.314	5.694	3.243	2.303
PSCEs	**−0.088** **−1.4%**	**−0.044** **−0.8%**	**−0.006** **−0.2%**	**0.010** **0.4%**
SRSH/PBE	7.901	6.621	2.933	2.588
SRSH/SRSH	8.008	6.688	2.935	2.581
PSCEs	**−0.107** **−1.3%**	**−0.067** **−1.0%**	**−0.003** **−0.1%**	**0.007** **0.3%**
Expt. [64]	8.4	6.5	3.0 [65]	2.5

We also studied the PSCEs when computing the equilibrium lattice parameters a_0, bulk moduli k_0, and atomization energies ΔE of MgO and AlP, which are the simplest (cubic) systems in Table I (see Sec. IV D in the Supplemental Material [41] for computational details). From the results shown in Table II, equilibrium lattice parameters are the least sensitive to DFA choice and PS consistency. While the computed atomization energies were not very sensitive to the DFA choice, this property has an average PSCE of -0.6% (or 24 meV/atom) for MgO and AlP [and a maximum PSCE of -0.7% (or 28 meV/atom) for AlP]. For the bulk moduli, we found an average PSCE in this response property of -0.5% (or 0.5 GPa) for MgO and AlP [and a maximum PSCE of -0.8% (or 0.7 GPa) for AlP]. We also note that the PSCEs when computing ΔE and k_0 were negative in all cases considered here; that is, the use of consistent DFA/PS combinations tends to yield larger values for these solid-state properties.

In general, our results agree with the general consensus that PSCEs tend to be smaller than the error due to the use

TABLE II. Equilibrium lattice parameters a_0 (Å), bulk moduli k_0 (GPa), and atomization energies ΔE (eV/atom) of select materials computed using consistent and inconsistent DFA/PS combinations. Absolute and relative PS consistency errors (PSCEs; bold font) were computed as property-specific differences between inconsistent and consistent DFA/PS combinations (i.e., PBE0/PBE versus PBE0/PBE0).

	MgO			AlP		
DFA/PS	a_0	k_0	ΔE	a_0	k_0	ΔE
PBE/PBE	4.272	147.4	4.741	5.515	81.7	4.118
PBE0/PBE	4.221	164.5	4.703	5.484	89.7	4.099
PBE0/PBE0	4.220	164.9	4.730	5.477	90.4	4.127
PSCEs	**0.001**	**−0.4**	**−0.027**	**0.007**	**−0.7**	**−0.028**
	0.0%	**−0.2%**	**−0.6%**	**0.1%**	**−0.8%**	**−0.7%**
HSE/PBE	4.222	163.9	4.718	5.485	89.2	4.106
HSE/HSE	4.222	164.2	4.744	5.479	89.8	4.131
PSCEs	**0.000**	**−0.3**	**−0.026**	**0.006**	**−0.6**	**−0.024**
	0.0%	**−0.2%**	**−0.5%**	**0.1%**	**−0.7%**	**−0.6%**
SRSH/PBE	4.205	170.5	4.703	5.486	89.1	4.103
SRSH/SRSH	4.207	170.7	4.723	5.479	89.7	4.129
PSCEs	**−0.002**	**−0.2**	**−0.020**	**0.006**	**−0.6**	**−0.025**
	0.0%	**−0.1%**	**−0.4%**	**0.1%**	**−0.7%**	**−0.6%**
Expt. [68]	4.19	165.0	5.20	5.45	86.0	4.32

of different DFAs [30,32,66]. While the PSCEs shown above are non-negligible and can reach 1.4% (or 0.1 eV) in the case of band gap calculations, this work further quantifies the errors made when using hybrid or RSH DFAs in conjunction with commonly available PBE-based PSs to compute a number of solid-state properties. Here, we emphasize that PSCEs are completely avoidable errors, especially when performing electronic structure calculations at the more demanding hybrid and RSH levels, and this work remedies this long-standing issue. We also note in passing that better agreement with the experimental values in Tables I and II can be obtained using a multiprojector PS, e.g., the optimized norm-conserving Vanderbilt (ONCV) pseudopotential method [67]; since this matter is not directly related to PSCEs, it was not pursued any further in this work.

IV. CONCLUSIONS AND FUTURE OUTLOOK

In this work, we presented a methodology for generating RSH-type PSs and a respective implementation in OPIUM. With the current implementation, any RSH functional can be used for PS generation. As a proof of principle, we generated nonlocal PSs for several atoms with GGA, hybrid, and RSH functionals. We tested the importance of PS consistency when computing a series of solid-state properties (e.g., band gaps, equilibrium lattice parameters, bulk moduli, and atomization energies) of MgO, AlN, TiO_2, and AlP. In doing so, our findings demonstrate that PSCEs are non-negligible (with an average of 0.4%) and can be as large as 1.4% (or 0.1 eV) when computing band gaps using inconsistent (but commonly available) PBE-based PSs. Equilibrium lattice parameters, bulk moduli, and atomization energies are somewhat less affected, with maximum PSCEs of 0.0% (0.002 Å), 0.8% (0.7 GPa), and 0.7% (28 meV/atom), respectively. We also observed that PSCEs tend to be systematic (i.e., most of the PSCE values are negative). As such, this work removes the need to incur these unnecessary errors when performing electronic structure calculations at the more demanding hybrid and RSH levels.

For further improvement, we plan on employing the multiprojector method [67], which has been shown to improve the results over standard KB design, for the hybrid and RSH PSs. In addition, we believe that the importance of using a consistent functional for the electronic structure calculation and underlying PS will be even more pronounced in at least two directions, i.e., response properties and heavier elements, both of which are known to be more sensitive to the basis set and PS [52,69]. In this regard, further improvements to hybrid (and RSH) functional codes [70–80] as well as extensions of the RSH and hybrid PS kernels to the projector augmented wave method [81] and scalar/fully relativistic PS generation schemes [82–84] will also be needed to explore these directions.

ACKNOWLEDGMENTS

The theoretical and computational research of T.Q., A.M.S., and A.M.R. was supported by the U.S. Department of Energy, Office of Science, Office of Basic Energy Sciences, under Award No. DE-FG02-07ER46431. L.K. was supported by the Israel Science Foundation, the Aryeh and Mintzi Katzman Professorial Chair, and the Helen and Martin Kimmel Award for Innovative Investigation. G.P. and Y.Y. acknowledge support from the Prof. Rahamimoff Travel Grants for Young Scientists program supported by the United States–Israel Binational Science Foundation. This material is based on work supported by the National Science Foundation under Grant No. CHE-1945676. R.A.D. also gratefully acknowledges financial support from an Alfred P. Sloan Research Fellowship. This research used resources of the National Energy Research Scientific Computing Center (NERSC), a U.S. Department of Energy Office of Science User Facility located at Lawrence Berkeley National Laboratory, operated under Contract No. DE-AC02-05CH11231.

[1] R. M. Dreizler and E. K. Gross, *Density Functional Theory: An Approach to the Quantum Many-Body Problem* (Springer, Berlin, 1990).

[2] R. G. Parr and W. Yang, *Density-Functional Theory of Atoms and Molecules* (Oxford University Press, New York, 1995).

[3] W. Koch and M. C. Holthausen, *A Chemist's Guide to Density Functional Theory*, 2nd ed. (Wiley-VCH, Weinheim, 2001).

[4] C. J. Cramer, *Essentials of Computational Chemistry: Theories and Models*, 2nd ed. (Wiley, Chichester, UK, 2004).

[5] P. Huang and E. A. Carter, Annu. Rev. Phys. Chem. **59**, 261 (2008).

[6] D. S. Sholl and J. A. Steckel, *Density Functional Theory: A Practical Introduction* (Wiley, Hoboken, NJ, 2009).

[7] F. Giustino, *Materials Modelling Using Density Functional Theory: Properties and Predictions* (Oxford University Press, Oxford, 2014).

[8] R. J. Maurer, C. Freysoldt, A. M. Reilly, J. G. Brandenburg, O. T. Hofmann, T. Björkman, S. Lebègue, and A. Tkatchenko, Annu. Rev. Mater. Res. **49**, 1 (2019).

[9] J. P. Perdew and K. Schmidt, in *Density Functional Theory and Its Application to Materials*, AIP Conf. Proc. No. 577 (AIP, Melville, NY, 2001), pp. 1–20.

[10] J. P. Perdew, K. Burke, and M. Ernzerhof, Phys. Rev. Lett. **77**, 3865 (1996).

[11] S. Kümmel and L. Kronik, Rev. Mod. Phys. **80**, 3 (2008).

[12] A. D. Becke, J. Chem. Phys. **98**, 1372 (1993).

[13] A. D. Becke, J. Chem. Phys. **98**, 5648 (1993).

[14] J. P. Perdew, M. Ernzerhof, and K. Burke, J. Chem. Phys. **105**, 9982 (1996).

[15] C. Adamo and V. Barone, J. Chem. Phys. **110**, 6158 (1999).

[16] A. Savin and H.-J. Flad, Int. J. Quantum Chem. **56**, 327 (1995).

[17] T. Leininger, H. Stoll, H.-J. Werner, and A. Savin, Chem. Phys. Lett. **275**, 151 (1997).

[18] A. V. Krukau, O. A. Vydrov, A. F. Izmaylov, and G. E. Scuseria, J. Chem. Phys. **125**, 224106 (2006).

[19] M. A. Rohrdanz and J. M. Herbert, J. Chem. Phys. **129**, 034107 (2008).

[20] E. Livshits and R. Baer, Phys. Chem. Chem. Phys. **9**, 2932 (2007).

[21] M. A. Rohrdanz, K. M. Martins, and J. M. Herbert, J. Chem. Phys. **130**, 054112 (2009).

[22] T. Yanai, D. P. Tew, and N. C. Handy, Chem. Phys. Lett. **393**, 51 (2004).

[23] J.-D. Chai and M. Head-Gordon, J. Chem. Phys. **128**, 084106 (2008).

[24] L. Kronik, T. Stein, S. Refaely-Abramson, and R. Baer, J. Chem. Theory Comput. **8**, 1515 (2012).

[25] L. Kronik and S. Kümmel, Adv. Mater. **30**, 1706560 (2018).

[26] W. E. Pickett, Comput. Phys. Rep. **9**, 115 (1989).

[27] J. R. Chelikowsky and M. L. Cohen, in *Basic Properties of Semiconductors*, Handbook on Semiconductors, edited by P. T. Landsberg (Elsevier, Amsterdam, 1992), Vol. 1, Chap. 3, pp. 59–111.

[28] D. J. Singh and L. Nordström, *Planewaves, Pseudopotentials, and the LAPW Method*, 2nd ed. (Springer, New York, 2005).

[29] P. Schwerdtfeger, ChemPhysChem **12**, 3143 (2011).

[30] M. Fuchs, M. Bockstedte, E. Pehlke, and M. Scheffler, Phys. Rev. B **57**, 2134 (1998).

[31] Y. Yao and Y. Kanai, J. Chem. Phys. **146**, 224105 (2017).

[32] J. Yang, L. Z. Tan, and A. M. Rappe, Phys. Rev. B **97**, 085130 (2018).

[33] A. P. Bartók and J. R. Yates, Phys. Rev. B **99**, 235103 (2019).

[34] J. C. Slater, *Quantum Theory of Atomic Structure* (McGraw-Hill, New York, 1960).

[35] C. Froese Fischer, *The Hartree–Fock Method for Atoms: A Numerical Approach* (Wiley, New York, 1977).

[36] J. G. Ángyán, I. Gerber, and M. Marsman, J. Phys. A **39**, 8613 (2006).

[37] OPIUM, https://opium.sourceforge.net.

[38] A. Seidl, A. Görling, P. Vogl, J. A. Majewski, and M. Levy, Phys. Rev. B **53**, 3764 (1996).

[39] T. M. Henderson, B. G. Janesko, and G. E. Scuseria, J. Chem. Phys. **128**, 194105 (2008).

[40] E. Weintraub, T. M. Henderson, and G. E. Scuseria, J. Chem. Theory Comput. **5**, 754 (2009).

[41] See Supplemental Material at http://link.aps.org/supplemental/10.1103/PhysRevB.108.165142 for a review of Slater's configuration-averaging (SCA) scheme, a detailed derivation of the SCA extensions needed for global and range-separated hybrid (RSH) functionals, a detailed derivation of the radial integro-differential equation for RSH self-consistent field calculations and implementation details, and computational details to accompany all calculations performed in this work. It also contains Refs. [85–90].

[42] S. Lehtola, Phys. Rev. A **101**, 012516 (2020).

[43] D. R. Hamann, M. Schlüter, and C. Chiang, Phys. Rev. Lett. **43**, 1494 (1979).

[44] A. M. Rappe, K. M. Rabe, E. Kaxiras, and J. D. Joannopoulos, Phys. Rev. B **41**, 1227 (1990); **44**, 13175 (1991).

[45] N. Troullier and J. L. Martins, Phys. Rev. B **43**, 1993 (1991).

[46] K. F. Garrity, J. W. Bennett, K. M. Rabe, and D. Vanderbilt, Comput. Mater. Sci. **81**, 446 (2014).

[47] M. van Setten, M. Giantomassi, E. Bousquet, M. Verstraete, D. Hamann, X. Gonze, and G.-M. Rignanese, Comput. Phys. Commun. **226**, 39 (2018).

[48] J. R. Trail and R. J. Needs, J. Chem. Phys. **122**, 014112 (2005).

[49] E. Engel, A. Höck, R. N. Schmid, R. M. Dreizler, and N. Chetty, Phys. Rev. B **64**, 125111 (2001).

[50] W. A. Al-Saidi, E. J. Walter, and A. M. Rappe, Phys. Rev. B **77**, 075112 (2008).

[51] N. J. Ramer and A. M. Rappe, Phys. Rev. B **59**, 12471 (1999).

[52] I. Grinberg, N. J. Ramer, and A. M. Rappe, Phys. Rev. B **63**, 201102(R) (2001).

[53] I. Grinberg, N. J. Ramer, and A. M. Rappe, in *The 11th Williamsburg Workshop on Fundamental Physics of Ferroelectrics*, AIP Conf. Proc. No. 582 (AIP, Melville, NY, 2001), p. 211.

[54] L. Kleinman and D. M. Bylander, Phys. Rev. Lett. **48**, 1425 (1982).

[55] X. Gonze, P. Käckell, and M. Scheffler, Phys. Rev. B **41**, 12264 (1990).

[56] X. Gonze, R. Stumpf, and M. Scheffler, Phys. Rev. B **44**, 8503 (1991).

[57] Y. Yang, G. Prokopiou, J. Yang, A. M. Rappe, L. Kronik, and R. A. DiStasio, Jr. (unpublished).

[58] H. Yukawa, Proc. Phys. Math. Soc. Jpn. **17**, 48 (1935).

[59] Y. Akinaga and S. Ten-no, Chem. Phys. Lett. **462**, 348 (2008).

[60] F. Tran and P. Blaha, Phys. Rev. B **83**, 235118 (2011).

[61] M. Seth and T. Ziegler, J. Chem. Theory Comput. **8**, 901 (2012).

[62] L. Kronik and J. B. Neaton, Annu. Rev. Phys. Chem. **67**, 587 (2016).

[63] P. Giannozzi *et al.*, J. Phys.: Condens. Matter **29**, 465901 (2017).

[64] D. Wing, G. Ohad, J. B. Haber, M. R. Filip, S. E. Gant, J. B. Neaton, and L. Kronik, Proc. Natl. Acad. Sci. USA **118**, e2104556118 (2021).

[65] M. Landmann, E. Rauls, and W. G. Schmidt, J. Phys.: Condens. Matter **24**, 195503 (2012).

[66] P. Borlido, J. Doumont, F. Tran, M. A. L. Marques, and S. Botti, J. Chem. Theory Comput. **16**, 3620 (2020).
[67] D. R. Hamann, Phys. Rev. B **88**, 085117 (2013) **95**, 239906(E) (2017).
[68] J. Harl, L. Schimka, and G. Kresse, Phys. Rev. B **81**, 115126 (2010).
[69] C. J. Pickard and F. Mauri, Phys. Rev. B **63**, 245101 (2001).
[70] S. Chawla and G. A. Voth, J. Chem. Phys. **108**, 4697 (1998).
[71] I. Duchemin and F. Gygi, Comput. Phys. Commun. **181**, 855 (2010).
[72] F. Gygi and I. Duchemin, J. Chem. Theory Comput. **9**, 582 (2013).
[73] L. Lin, J. Chem. Theory Comput. **12**, 2242 (2016).
[74] S. Mandal, J. Debnath, B. Meyer, and N. N. Nair, J. Chem. Phys. **149**, 144113 (2018).
[75] S. Mandal and N. N. Nair, J. Chem. Phys. **151**, 151102 (2019).
[76] S. Mandal and N. N. Nair, J. Comput. Chem. **41**, 1790 (2020).
[77] H.-Y. Ko, J. Jia, B. Santra, X. Wu, R. Car, and R. A. DiStasio, Jr., J. Chem. Theory Comput. **16**, 3757 (2020).
[78] S. Mandal, V. Thakkur, and N. N. Nair, J. Chem. Theory Comput. **17**, 2244 (2021).
[79] H.-Y. Ko, B. Santra, and R. A. DiStasio, Jr., J. Chem. Theory Comput. **17**, 7789 (2021).
[80] H.-Y. Ko, M. F. Calegari Andrade, Z. M. Sparrow, J. Zhang, and R. A. DiStasio, Jr., J. Chem. Theory Comput. **19**, 4182 (2023).
[81] P. E. Blöchl, Phys. Rev. B **50**, 17953 (1994).
[82] L. Kleinman, Phys. Rev. B **21**, 2630 (1980).
[83] I. Grinberg, N. J. Ramer, and A. M. Rappe, Phys. Rev. B **62**, 2311 (2000).
[84] M. Dolg and X. Cao, Chem. Rev. **112**, 403 (2012).
[85] A. Messiah, *Quantum Mechanics: Two Volumes Bound as One* (Dover, Mineola, NY, 1999).
[86] E. Aprà *et al.*, J. Chem. Phys. **152**, 184102 (2020).
[87] B. Lee, C.-K. Lee, C. S. Hwang, and S. Han, Curr. Appl. Phys. **11**, S293 (2011).
[88] A. Jain, S. P. Ong, G. Hautier, W. Chen, W. D. Richards, S. Dacek, S. Cholia, D. Gunter, D. Skinner, G. Ceder, and K. A. Persson, APL Mater. **1**, 011002 (2013).
[89] T. Björkman, Comput. Phys. Commun. **182**, 1183 (2011).
[90] F. D. Murnaghan, Proc. Natl. Acad. Sci. USA **30**, 244 (1944).